# Intrinsic toroidal rotation in the scrape-off layer of tokamaks

J. Loizu, P. Ricci, F. D. Halpern, S. Jolliet, and A. Mosetto

Citation: Physics of Plasmas (1994-present) **21**, 062309 (2014); doi: 10.1063/1.4883498
View online: http://dx.doi.org/10.1063/1.4883498
View Table of Contents: http://scitation.aip.org/content/aip/journal/pop/21/6?ver=pdfcov
Published by the AIP Publishing



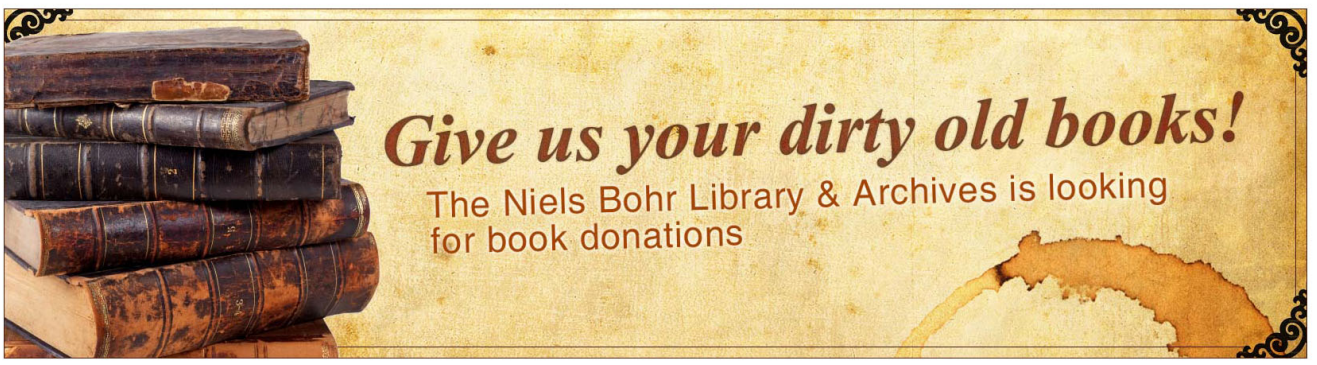

# Intrinsic toroidal rotation in the scrape-off layer of tokamaks

J. Loizu,[a] P. Ricci, F. D. Halpern, S. Jolliet, and A. Mosetto
*Centre de Recherches en Physique des Plasmas (CRPP), École Polytechnique Fédérale de Lausanne (EPFL), CH-1015 Lausanne, Switzerland*

(Received 26 February 2014; accepted 26 May 2014; published online 18 June 2014)

The origin and nature of intrinsic toroidal plasma rotation in the scrape-off-layer (SOL) of tokamaks is investigated both analytically and through numerical simulations. It is shown that the equilibrium poloidal $E \times B$ flow, the sheath physics, and the presence of poloidal asymmetries in the pressure profile act as sources of momentum, while turbulence provides the mechanism for the radial momentum transport. An equation for the radial and poloidal dependence of the equilibrium parallel ion flow is derived, and a simple analytical solution is presented. This solution reproduces and explains the main experimental trends for the Mach number found in the SOL of tokamaks. Global, three-dimensional fluid simulations of SOL turbulence in different limiter configurations confirm the validity of the analytical theory. [http://dx.doi.org/10.1063/1.4883498]

## I. INTRODUCTION

Tokamak plasmas have been observed to spontaneously rotate toroidally even in the absence of momentum injection.[1–3] As sufficiently large rotation has been shown to stabilize MHD instabilities[4,5] and reduce turbulent transport,[6] understanding the origin and nature of intrinsic toroidal rotation is of special importance for future fusion devices such as ITER where the effective deposition of momentum is expected to be small.[7,8] While the experimental and theoretical research effort has mostly focused on toroidal rotation inside the Last Closed Flux Surface (LCFS),[9–20] there is strong experimental evidence for the role of the Scrape-Off Layer (SOL) in determining core rotation profiles.[21] This is consistent with the idea that any source of net toroidal momentum must come from the boundary, as implied by the momentum conservation law.[22] Recently, it was also found that strong flows in the SOL set the boundary conditions on the confined plasma and can even determine the low-to-high confinement mode power threshold.[23] While some theoretical and numerical studies have focused on SOL rotation driven by classical flows,[24,25] a revealing description of the phenomena that takes into account the fundamental elements of the SOL, such as turbulent momentum transport and plasma sheaths, is still lacking. This is particularly important since, as experimental data reveal,[21] explaining parallel flows requires a detailed description of turbulent transport.

Typically, the toroidal Mach number in the SOL of L-mode plasmas is measured to be of order one and in the co-current direction, even when the toroidal magnetic field[26] or the total magnetic field[23] is reversed. This can be qualitatively explained by the recirculation of classical flows ($\mathbf{E} \times \mathbf{B}$, diamagnetic, or Pfirsch-Schlüter) in the parallel direction. It has been observed, nevertheless, that the magnitude and direction of toroidal rotation are not exactly invariant with respect to magnetic field reversal: rotation can become stronger or weaker in the co-current direction,[23,26] and under certain conditions it can even become counter-current.[27] Similar behavior has been observed when the plasma is brought from a lower single null to an upper single null configuration.[23] These observations have been related to the presence of transport asymmetries. It remains unclear, however, how recirculation of classical flows and transport asymmetries combine together and give rise to the observed toroidal Mach number profiles in the many different magnetic configurations explored experimentally. This is also reflected by the fact that a theory is missing able to describe all these effects simultaneously.

In this paper, the origin and nature of intrinsic toroidal plasma rotation in the SOL of tokamaks is investigated both analytically and through numerical simulations. We start by showing that there is a net volume-averaged toroidal flow in global simulations of SOL turbulence despite the fact that no momentum is injected, therefore, implying that there are intrinsic toroidal flows established in the SOL. In order to understand the origin of such flows, we provide an analytical description of the generation and transport of toroidal plasma rotation in the SOL, based on the plasma momentum balance, the turbulent transport, and the sheath boundary conditions. Results suggest that the equilibrium (i.e., time-average) poloidal $\mathbf{E} \times \mathbf{B}$ flow, the sheath physics, and the presence of poloidal asymmetries in the pressure profile act as sources of parallel flow, while turbulence provides the mechanism for the radial momentum transport. We first derive an equation describing the radial and poloidal dependence of the equilibrium parallel flow by providing, for the first time, a first-principle based estimate of the turbulent momentum transport in the SOL. Second, we present an approximate analytical solution of the equation that describes the toroidal rotation profile in the poloidal plane. Then, the result of global, three-dimensional turbulence simulations of a limited SOL are presented, showing good agreement with our theory. Finally, a first attempt to compare the theoretical predictions with experimental measurements is presented. We show that the analytical solution reproduces fairly well experimental trends for the direction and magnitude of toroidal rotation. In particular, results indicate that intrinsic rotation is co-current most of the time but can be reversed due to pressure asymmetries under certain conditions that are consistent with those observed in tokamaks.

[a]Electronic address: joaquim.loizu@ipp.mpg.de

This paper is organized as follows. In Sec. II, we show examples of three-dimensional turbulence simulations that illustrate the existence of SOL intrinsic flows and motivate the need for a theory that takes into account the physics of turbulent transport. Such theory is the subject of Sec. III. In Sec. IV, the analytical results for the toroidal Mach number profile are contrasted with the results of SOL turbulence simulations in different limited configurations. A comparison between the theoretical predictions and the observed experimental trends is presented in Sec. V. The conclusions and outlook follow in Sec. VI.

## II. INTRINSIC FLOWS IN SOL SIMULATIONS

In this section, we show that intrinsic flows are present in simulations of SOL turbulence. We carry out these simulations with the GBS (Global Braginskii Solver) code, a two-fluid code based on the drift-reduced Braginskii equations, capable of performing global, three-dimensional, full- $n$, flux-driven simulations of SOL turbulence.[28] These simulations can explore the self-consistent evolution and structure of the plasma profiles in the presence of (i) plasma density and heat input from the core of the fusion machine, (ii) cross-field transport produced by plasma instabilities (interchange instability or drift waves, for example), and (iii) parallel losses at the sheaths where the magnetic field lines terminate on the walls. We would like to remark that a fluid description of the SOL dynamics with a model based on the Braginskii equations may be limited to low-temperature regimes such as the L-mode. In fact, high-temperature events, such as the Edge Localized Modes (ELMs) observed in H-mode plasmas,[29] may require more sophisticated fluid closures.[30] As an example, we consider here the result of a simulation of SOL electrostatic turbulence in the simplest case of circular magnetic flux surfaces and a toroidal limiter on the high field side (Figure 1). The corresponding equations solved by GBS are shown in Appendix A, together with the magnetic presheath boundary conditions imposed at the end of the field lines. Although no momentum is injected into the system, a careful inspection of the equilibrium

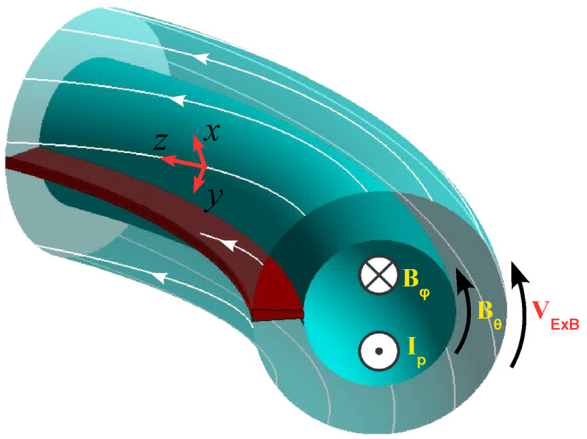


FIG. 1. Sketch of the SOL geometry with its magnetic topology. The directions of the toroidal magnetic field $B_\varphi$, the poloidal magnetic field $B_\theta$, and that of the corresponding plasma current $I_p$ are indicated. Also the expected direction of the equilibrium $\mathbf{E}\times\mathbf{B}$ flow is shown.

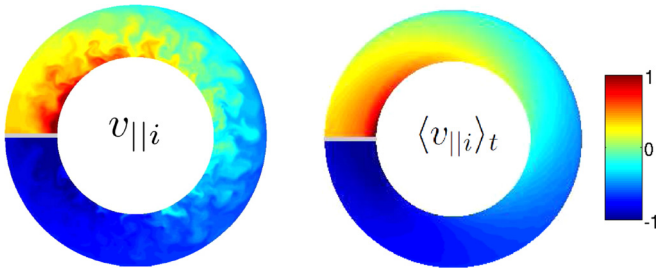


FIG. 2. Snapshot (left) and time-average (right) of the parallel ion velocity in a poloidal cross-section of the tokamak SOL. Results are obtained from GBS simulations with the following model parameters: major radius $R=500\hat{\rho}_s$, inverse aspect ratio $a/R\approx 0.25$, radial extension $L_x=x_{max}-x_{min}=100\hat{\rho}_s$, safety factor $q=4$, mass ratio $m_i/m_e=200$, sheath coefficient $\Lambda=3$, parallel resistivity $\nu_\parallel=0.1\hat{\nu}$, parallel heat diffusivity $\chi_{\parallel e}=\hat{\chi}$, and viscosity $\eta_{0e}=\hat{\eta}$. The pitch angle of the magnetic field is such that $\tan\alpha=a/qR\approx 0.0625$, corresponding to $\alpha\approx 3.6^\circ$. The particle and heat outflow from the core is modeled by density and temperature Gaussian sources that are radially-localized at $x=x_s=x_{min}+30\hat{\rho}_s$ and have a width of $5\hat{\rho}_s$. The snapshot covers a radial extension $(x_s, x_{max})$. We assume no magnetic shear, infinite aspect ratio, and cold ions.

parallel ion velocity reveals the existence of a net volume-averaged parallel flow. Figure 2 shows a snapshot of the ion parallel velocity, $V_{||i}$, and its toroidal and time-average, $\bar{V}_{||i}$, in a poloidal cross-section. Since the pitch angle $\alpha=a/qR$ of the magnetic field is very small, $\alpha\ll 1$, $\bar{V}_{||i}$ represents to a very good approximation the toroidal rotation. According to the magnetic presheath boundary conditions, plasma outflows from the system at the limiter. Therefore, $V_{||i}$ is positive on the top side of the limiter, where the magnetic field is directed towards the wall, and negative on the bottom side of the limiter, where the opposite situation applies (Figure 1). However, as Fig. 2 shows, the zero of $\bar{V}_{||i}$ is not half way between the two faces of the limiter, namely at $\theta=0$. Instead, the SOL region where $\bar{V}_{||i}<0$ is larger than the $\bar{V}_{||i}>0$ region, and a volume-average of $\bar{V}_{||i}$ gives a value of approximately $-0.3c_s$. Given the direction of the toroidal and poloidal components of the magnetic field, we conclude that the negative, net parallel flow corresponds to a toroidal plasma rotation in the co-current direction, i.e., in the direction of the plasma current $I_p$ (see Fig. 1). We would like to notice that a conservation law for the total toroidal momentum can be derived from the drift-reduced fluid equations solved by GBS (see Appendix B). In particular, Eq. (B5) shows that the source of intrinsic toroidal flow in the SOL is determined both by the flow and pressure differences between the two ends of the field lines, thus strongly regulated by the sheath physics.

We now give a qualitative explanation for the origin of this net co-current flow, based on the effect that the sheath has on the parallel ion velocity. Since the equilibrium radial electric field in the SOL is positive,[31] $E_x>0$, a stationary poloidal $\mathbf{E}\times\mathbf{B}$ flow is directed from the bottom side of the limiter to its top side (Fig. 1). As discussed in Ref. 32, the poloidal $\mathbf{E}\times\mathbf{B}$ flow is recirculated at the magnetic presheath entrance in the parallel direction, in such a way that the ion flow perpendicular to the wall does not depend on the value of the $\mathbf{E}\times\mathbf{B}$ flow. More precisely, at the magnetic presheath entrance, the parallel ion velocity, Eq. (A12), is approximately given by

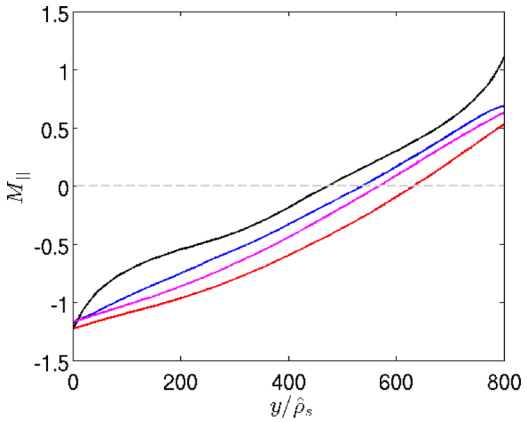


FIG. 3. Poloidal profiles of the equilibrium parallel Mach number, $M_{||} = \bar{V}_{||i}/\bar{c}_s$, at different radial locations: at the source position $x_s = 30\hat{\rho}_s$ (black), and at $x = 50\hat{\rho}_s$ (blue), $x = 70\hat{\rho}_s$ (magenta), and $x = 90\hat{\rho}_s$ (red). Results are obtained from GBS simulations with a limiter on the HFS midplane.

$$V_{||i} \simeq c_s \left[ \pm 1 - \frac{\Lambda}{\alpha} \frac{\rho_s}{L_\phi} \right], \tag{1}$$

where $L_\phi$ is the equilibrium radial scale length of $\phi$, and we have assumed $e\phi \sim \Lambda T_e$ at the magnetic presheath entrance. The terms related to density and temperature gradients have been omitted here, as they lead to smaller corrections than the term related to $\phi$. The deviation from the sound speed in Eq. (1) is of order one for typical SOL conditions. In our simulation, which is representative of typical SOL experimental parameters, $\Lambda\rho_s/(\alpha L_\phi) \approx 0.5$, since $\Lambda = 3$, $\alpha = 3.6^\circ$, and $L_\phi \approx 100\rho_s$. Namely, the parallel flows at the bottom and top sides of the limiter are expected to be supersonic and subsonic, respectively. This is confirmed by Fig. 3, which shows the poloidal profiles of the equilibrium parallel Mach number, $M_{||} = \bar{V}_{||i}/\overline{c_s}$, at different radial locations. Moreover, we observe that the profiles are fairly linear and thus almost entirely determined by the boundary conditions. This implies the presence of a negative, net parallel flow as given by the deviation from the sound speed at the boundaries. We remark that there is an asymmetry in the deviation of $\bar{V}_{||i}$ from $\overline{c_s}$, if one compares the two sides of the limiter. This is due to the different radial profiles of $\bar{\phi}$ established at the top and bottom sides of the limiter (data not shown).

However, the simple picture of the sheath boundary condition offsetting a linear poloidal profile of $\bar{V}_{||i}$ cannot be always used to describe intrinsic flows in the SOL. Figure 4 shows the results of a simulation carried out with the same parameters as in Fig. 2 but with the limiter on the bottom of the tokamak. For this configuration, the volume-average of $\bar{V}_{||i}$ gives a value of approximately $-0.05c_s$, hence the net flow is almost zero, much smaller than in the high field side (HFS)-limited case. This is despite the fact that the parallel flows at the left and right sides of the limiter are, as before, respectively subsonic and supersonic, with deviations from the sound speed comparable to the previous case. The reason is that the profiles of $M_{||}$ are no longer linearly dependent on the poloidal angle, as shown in Fig. 5. As shown later, other mechanisms such as the turbulent momentum transport, compete with the effect of the sheath in determining the rotation profile, such that the resulting net flow is close to zero.

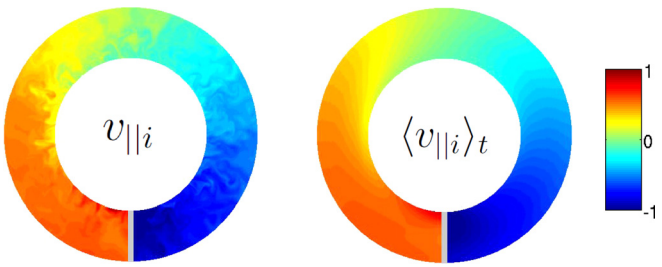


FIG. 4. Snapshot (left) and time-average (right) of the parallel ion velocity in a poloidal cross-section of the tokamak SOL. Results are obtained from GBS simulations. The simulation parameters are the same as in Fig. 2 but with the limiter on the bottom of the vessel.

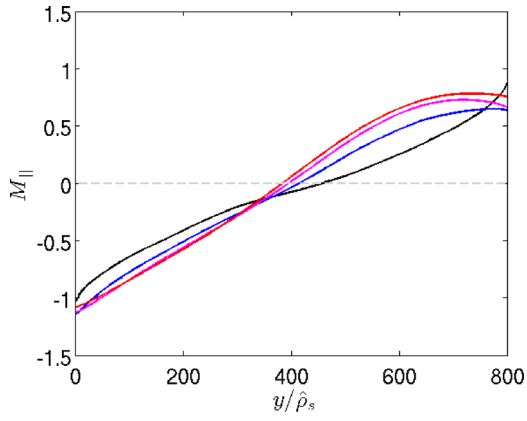


FIG. 5. Poloidal profiles of the equilibrium parallel Mach number, $M_{||} = \bar{V}_{||i}/\bar{c}_s$, at different radial locations: at the source position $x_s = 30\hat{\rho}_s$ (black), and at $x = 50\hat{\rho}_s$ (blue), $x = 70\hat{\rho}_s$ (magenta), and $x = 90\hat{\rho}_s$ (red). Results are obtained from GBS simulations. The simulation parameters are the same as in Fig. 2 but with the limiter located on the bottom of the vessel.

These observations motivate the analytical study of SOL parallel flows in a more general framework that includes, in particular, the description of turbulent momentum transport, conservation of momentum, and sheath boundary conditions. This study is the subject of Sec. III.

## III. THEORY OF INTRINSIC ROTATION IN THE SOL

In this section, we provide an analytical description of the generation and transport of toroidal plasma rotation in the SOL, based on the plasma momentum balance, the turbulent transport, and the sheath boundary conditions. We derive an equation describing the radial and poloidal dependence of the equilibrium parallel flow by providing, for the first time, a first-principle based estimate of the turbulent momentum transport in the SOL.

An electrostatic drift-reduced fluid model is suitable to describe the SOL[33,34] and we use it here for the description of the plasma dynamics. In fact, the electron mean-free path is much smaller than the connection length, $\lambda_e \ll L_{||}$, and trapped particles play a minor role since $\nu^*_{i,e} \gg 1$.[35] Also, electrostatic low-frequency turbulence at small wave number, $\omega \ll \omega_{ci}$, $k_\perp \rho_s < 1$ and $k_{||} L_{||} \sim 1$, is believed to dominate the cross-field transport of particles and heat in the SOL, mainly driven by interchange-like modes such as resistive

ballooning modes.[27] Such modes are also responsible for the turbulent momentum transport that arises from the presence of sheared parallel flows, namely when $\partial_x M_{||} \neq 0$.

### A. Two-dimensional equation for the equilibrium toroidal flow

Let us describe the SOL of a tokamak of major radius $R$ by using a right-handed system of coordinates $(y, x, \varphi)$, where $\varphi$ is the toroidal coordinate (counterclockwise direction when looking from the top) and $(x, y)$ define the plane perpendicular to the magnetic field $\mathbf{B}$. The coordinate $x$ is a flux coordinate and extends over the full SOL width, with $x=0$ at the separatrix. The coordinate $y$ is perpendicular to $x$ and $\mathbf{B}$ and follows the open flux surfaces, with $y=0$ half way from the two limiter sides or divertor plates, going from $y=-L_y/2$ to $y=L_y/2$. In a circular plasma with infinite aspect ratio, $x$ and $y$ correspond to the radial and poloidal coordinates, respectively. The equilibrium magnetic field can be written as $\mathbf{B} = |B_\varphi|\left(\sigma_\varphi \hat{\mathbf{e}}_\varphi + \alpha\sigma_\theta \hat{\mathbf{e}}_\theta\right)$, where $\alpha = |B_\theta/B_\varphi|$ is the pitch angle and $\sigma_{\varphi,\theta} = \pm 1$ gives the orientation of the magnetic field in the toroidal and poloidal directions. For simplicity, we consider the large aspect ratio limit, therefore, the plane $(x, y)$ coincides with the poloidal plane. We also assume that the SOL width is much smaller than the tokamak minor radius.

Within a drift-reduced fluid model, the evolution of the parallel ion velocity can be obtained by summing the ion and electron parallel momentum equations and neglecting electron inertia,

$$\frac{\partial V_{||i}}{\partial t} + V_{||i}\nabla_{||} V_{||i} + (\mathbf{V}_E \cdot \nabla_\perp) V_{||i} + \frac{1}{m_i n}\nabla_{||} p = 0, \qquad (2)$$

where $p = p_e + p_i$ is the total scalar plasma pressure and $\mathbf{V}_E$ is the $\mathbf{E}\times\mathbf{B}$ velocity. We remark that the effect of finite ion temperature is included without accounting for finite Larmor radius effects. Equation (2) represents the conservation of plasma parallel momentum. A detailed derivation of Eq. (2) can be found, e.g., in Ref. 36. The absence of the ion diamagnetic drift in the convection of parallel momentum is due to the so-called diamagnetic cancellation which arises from the lowest order term in the pressure tensor, in the limit $L_\perp/R \ll 1$.[37] Also, we have neglected terms of order $\rho_i/L_\perp \ll 1$, $(k_\perp \rho_s)^2 \ll 1$, and $\tau_i \ll L_{||}/c_s$. Here $c_s = \sqrt{(T_e + T_i)/m_i}$ and $\tau_i$ is the characteristic time for momentum exchange under ion-ion collisions. Finally, we notice that in this paper we do not consider recycling, ionization or recombination processes, therefore the validity of the model presented herein may be limited to sheath-limited and low-recycling regimes.[38]

We now deduce from Eq. (2) an equation for the equilibrium parallel flow $\bar{V}_{||i}$ in the SOL. We will denote fluctuations with a tilde, and equilibrium with an overbar, e.g., $V_{||i} = \bar{V}_{||i} + \tilde{V}_{||i}$. Time-averaging Eq. (2) leads to

$$\bar{V}_{||i}\nabla_{||}\bar{V}_{||i} + \nabla_\perp \cdot \bar{\mathbf{\Gamma}} + \frac{1}{m_i \bar{n}}\nabla_{||}\bar{p} = 0. \qquad (3)$$

The cross-field momentum transport term has been written as a divergence of a flux, i.e., $(\mathbf{V}_E \cdot \nabla_\perp) V_{||i} = \nabla_\perp \cdot \mathbf{\Gamma}$, where

$$\Gamma_x = \frac{\sigma_\varphi}{|B_\varphi|}\frac{\partial \phi}{\partial y} v_{||i}, \qquad (4)$$

and

$$\Gamma_y = -\frac{\sigma_\varphi}{|B_\varphi|}\frac{\partial \phi}{\partial x} v_{||i} \qquad (5)$$

correspond to, respectively, the radial and poloidal fluxes of parallel ion velocity. In Eq. (3) we have assumed that $\overline{\tilde{V}_{||i}\nabla_{||}\tilde{V}_{||i}} \ll \bar{V}_{||i}\nabla_{||}\bar{V}_{||i}$ and similarly for the pressure term. This is justified because the ratio of the fluctuating and equilibrium terms is at most (if fluctuations correlate perfectly) of the order of $k_{||}L_{||}(\tilde{V}_{||i}/c_s)^2$, which is small in typical SOL conditions where $k_{||}L_{||} \sim 1$ and $\tilde{V}_{||i}/c_s \sim 0.1 - 0.5$.[39] Assuming toroidal axisymmetry, equilibrium quantities only depend on $x$ and $y$, thus we can replace $\nabla_{||}$ with $\alpha\sigma_\theta\partial_y$ and, therefore,

$$\alpha\sigma_\theta \bar{V}_{||i}\frac{\partial \bar{V}_{||i}}{\partial y} + \nabla_\perp \cdot \bar{\mathbf{\Gamma}} + \frac{\alpha\sigma_\theta}{m_i \bar{n}}\frac{\partial \bar{p}}{\partial y} = 0. \qquad (6)$$

The time-average of the radial momentum flux is the sum of a turbulent and an equilibrium term

$$\bar{\Gamma}_x = \Gamma_x^T + \Gamma_x^E = \frac{\sigma_\varphi}{|B_\varphi|}\overline{\tilde{V}_{||i}\frac{\partial \tilde{\phi}}{\partial y}} + \frac{\sigma_\varphi}{|B_\varphi|}\bar{V}_{||i}\frac{\partial \bar{\phi}}{\partial y}, \qquad (7)$$

and an analogous expression is valid for $\bar{\Gamma}_y$. We first evaluate $\Gamma_x^T$, by starting with the estimate of the fluctuations of the parallel ion velocity. Linearizing Eq. (2) around the equilibrium, and keeping the leading order terms, we have

$$\gamma \tilde{V}_{||i} \sim \frac{\sigma_\varphi}{|B_\varphi|}\frac{\partial \tilde{\phi}}{\partial y}\frac{\partial \bar{V}_{||i}}{\partial x}, \qquad (8)$$

where $\gamma$ is the linear growth rate of the mode dominating the transport. From Eq. (8), it follows $\Gamma_x^T \sim (\partial_y \tilde{\phi})^2$; we are thus led to estimate the amplitude of the poloidal electric field fluctuations. Linearizing the pressure continuity equation, which can be obtained by combining the density and temperature equations, and keeping the dominant terms, we have

$$\gamma \tilde{p} \sim \frac{\sigma_\varphi}{|B_\varphi|}\frac{\partial \tilde{\phi}}{\partial y}\frac{\partial \bar{p}}{\partial x}. \qquad (9)$$

It is possible to relate the pressure fluctuations $\tilde{p}$ with its equilibrium value $\bar{p}$ by assuming that the mode growth saturates when the fluctuations are able to remove the instability drive, which is provided by the pressure gradient, i.e. when $\partial_x \tilde{p} \sim \partial_x \bar{p}$. Numerical simulations show that this saturation mechanism can be used to accurately describe the properties of SOL turbulence.[34] Equation (9) can thus be written as

$$\frac{\sigma_\varphi}{|B_\varphi|}\frac{\partial \tilde{\phi}}{\partial y} \sim \frac{\gamma}{k_x}, \qquad (10)$$

where $k_x$ gives the radial extension of the saturated turbulent eddies. This can be estimated using non-local linear theory

as $k_x = \sqrt{k_y/L_p}$.[40] Combining Eqs. (8) and (10), we get an expression for the turbulent part of the time-averaged radial momentum flux

$$\Gamma_x^T = -\frac{\gamma}{k_y} L_p \frac{\partial \bar{V}_{||i}}{\partial x}. \tag{11}$$

At this point, we need to give an estimate of the ratio $\gamma/k_y$, which should be computed by using the values of $\gamma$ and $k_y$ of the modes that play the dominant role in the transport. As transport in the SOL is typically dominated by resistive ballooning modes,[27,33] one can use the corresponding ballooning growth rate $\gamma_b = c_s\sqrt{2/RL_p}$ and wavenumber $k_b = \sqrt{\omega_{ci}B/(\gamma_b q^2 R^2 e n \nu_{||})}$.[41] However, it is also possible to use the more general relation (see Appendix C for a derivation)

$$L_p \sim \frac{qR}{c_s}\frac{\gamma}{k_y}, \tag{12}$$

to express the ratio $\gamma/k_y$ as a function of $L_p$. This relation results from a pressure balance between parallel streaming and perpendicular turbulent transport, and has been shown to predict with high accuracy the pressure scale length $L_p$ in global simulations of SOL turbulence.[33] Also, Eq. (12) has been used to express $L_p$ as a function of the SOL operational parameters, showing good agreement with experimental data from a number of tokamaks.[42] By using Eq. (12), we can finally write the turbulent part of the time-averaged radial momentum flux, valid for all SOL turbulent regimes, as

$$\Gamma_x^T = -D_{turb}\frac{\partial \bar{V}_{||i}}{\partial x}, \tag{13}$$

where

$$D_{turb} = \frac{L_p^2 c_s}{qR} \tag{14}$$

results from the net momentum transport arising from saturated turbulence. An estimate of the order of magnitude of $D_{turb}$ for typical SOL parameters gives $D_{turb} \sim 1\ \mathrm{m^2\ s^{-1}}$. Notice that Eq. (13) is an expression that only involves equilibrium quantities, and that $D_{turb}$ can be written as a function of the SOL operational parameters. From Eq. (13), we can also evaluate the relative importance of the equilibrium and turbulent parts of the radial momentum transport. A rough estimate gives $\Gamma_x^E/\Gamma_x^T \sim \rho_s/L_p$, thus the radial momentum transport is mainly turbulent and we shall neglect the equilibrium contribution.

We now focus our attention on the time-average of the poloidal momentum turbulent flux. From Eq. (8), we have that $\Gamma_y^T \sim \overline{\partial_y\tilde{\phi}\partial_x\tilde{\phi}}$ which is expected to average to approximately zero. In fact, if the potential perturbation has the form $\tilde{\phi} = \tilde{\phi}_0(x)\exp\left[i(k_y y - \omega t)\right]$, where $\tilde{\phi}_0(x)$ describes the radial envelope of the mode, then $\overline{\partial_y\tilde{\phi}\partial_x\tilde{\phi}} = 0$. It follows that $\bar{\Gamma}_y \simeq \Gamma_y^E$ and Eq. (6) can finally be written as

$$-\frac{\partial}{\partial x}\left(D_{turb}\frac{\partial \bar{V}_{||i}}{\partial x}\right) - \frac{\sigma_\varphi}{|B_\varphi|}\frac{\partial \bar{\phi}}{\partial x}\frac{\partial \bar{V}_{||i}}{\partial y} + \alpha\sigma_\theta \bar{V}_{||i}\frac{\partial \bar{V}_{||i}}{\partial y} + \frac{\alpha\sigma_\theta}{m_i \bar{n}}\frac{\partial \bar{p}}{\partial y} = 0\,. \tag{15}$$

When taking the divergence of the flux, we have neglected the curvature term that arises from the variation of the magnetic field, as $R/L_\perp \gg 1$ in the SOL, and $\bar{V}_{||i}\partial_{xy}^2\bar{\phi}$ has been neglected with respect to $\partial_y \bar{V}_{||i}\partial_x\bar{\phi}$.

Equation (15) is a two-dimensional differential equation for the equilibrium parallel ion flow, $\bar{V}_{||i}(x,y)$, which describes the balance between radial diffusion due to the time-averaged turbulent transport (first term), poloidal convection (second term), parallel convection (third term), and momentum generation by the pressure force (fourth term). We remark that the radial dependence of $D_{turb}$ leads to a term that acts as an effective radial convection with velocity $v_{turb} = D_{turb}/2L_T > 0$, thus directed radially outwards. Here, $L_T^{-1} = |\partial_x(T_e + T_i)/(T_e + T_i)|^{-1}$ corresponds to the radial scale length of the temperature profile. In general, $D_{turb}$ may also have a poloidal dependence, $D_{turb}(\theta)$, e.g., due to the ballooning character of the turbulence.

The solution of Eq. (15) requires boundary conditions for $\bar{V}_{||i}$ in the radial direction, at the separatrix and at the vessel wall, and in the poloidal direction, at the limiter or divertor plates. The latter are given by the magnetic presheath entrance condition, Eq. (A12)

$$V_{||i}^{\pm} = \pm\sigma_\theta c_s^{\pm} + \left.\frac{\sigma_\theta\sigma_\varphi}{\alpha|B_\varphi|}\frac{\partial\phi}{\partial x}\right|^{\pm} \tag{16}$$

at $y = \pm L_y/2$, respectively (as before, the terms related to density and temperature gradients are neglected). We note that, as already discussed in Sec. II, the $\mathbf{E}\times\mathbf{B}$ drift correction in Eq. (16) introduces an asymmetry in the ion parallel flow between the two limiter sides or divertor plates, thus providing a mechanism for net toroidal flow generation.

Equation (15) can in principle be solved once $\bar{\phi}(x,y)$ and $\bar{p}(x,y)$ are known. While these two quantities have been studied in detail in Refs. 31, 42, and 43, their complete knowledge is not necessary to capture the main physics of rotation, and, as we show later, an estimate of those is enough to obtain a good understanding and a quantitative estimate of the toroidal rotation profiles.

### B. Solution for non-strongly poloidally localized transport

In this section, we derive an approximate analytical solution for $\bar{V}_{||i}(x,y)$, by assuming that the turbulent transport is not strongly localized in the poloidal direction. More precisely, we assume that even in the case of ballooned transport, the portion of poloidal angle in which the plasma is radially transported by turbulence is a non-negligible fraction of 360°. We remark that this has been suggested by measurements obtained on the ISTTOK[44] and Tore Supra[45] tokamaks, where the portion of poloidal angle is found to be of about 120° and 60°, respectively. Thus we assume $D_{turb}(x,\theta) = D_{turb}(x)$

in Eq. (15), while poloidal asymmetries still persist in the pressure force term.

We now make some further assumptions on the equilibrium profiles in order to progress analytically and find a solution $\bar{V}_{||i}(x,y)$ that satisfies Eq. (15) with boundary conditions given by Eq. (16). Let us assume that the equilibrium profiles can be Taylor expanded in the $y$ direction, so that

$$\bar{V}_{||i}(x,y) = u_0(x) + u_1(x)y + u_2(x)y^2 \tag{17}$$

and similarly for $\bar{p}(x,y)$ and $\bar{\phi}(x,y)$. This choice is justified by the following argument. The ion continuity equation is given by $\nabla_{||}(nV_{||i}) + \nabla_{\perp}\cdot(n\mathbf{V}_{\perp i}) = 0$, where the second term includes both the equilibrium and fluctuating $\mathbf{E}\times\mathbf{B}$ flows. Typically, in the literature,[21,38,46] the contribution of the Pfirsch-Schlüter ion flow is assumed to modulate the $\bar{V}_{||i}$ poloidal profile, leading to $\bar{V}_{||i}^{PS} \sim 2qV_E\cos\theta$. However, the contribution of turbulence in the continuity equation is larger by a factor

$$\frac{\text{Turbulence}}{\text{Pfirsch}-\text{Schlüter}} \sim \frac{D_{turb}\,\bar{n}/L_n^2}{\cos\theta\,\bar{n}V_E/R} \sim \frac{1}{q\cos\theta}\frac{c_s}{V_E} \sim \frac{1}{q\cos\theta}\frac{L_\perp}{\rho_s} \gg 1. \tag{18}$$

Therefore, if turbulence in the SOL does not have a strong poloidal dependence, as it has been revealed experimentally[44,45] and by numerical simulations of ballooning-mode driven turbulence,[47] also shown in Sec. IV, the continuity equation gives $\nabla_{||}(nV_{||i}) \sim const$ and thus a poloidal profile of $\bar{V}_{||i}$ close to linear, as taken into account in Eq. (17). We remark that this has also been concluded from multi-machine measurements of parallel flows.[48] Imposing the sheath boundary conditions, Eq. (16), we find the following constraints for the Taylor coefficients

$$u_1(x) = (\bar{V}_{||i}^{+} - \bar{V}_{||i}^{-})/L_y, \tag{19}$$

$$u_2(x) = 4(u_{sh} - u_0(x))/L_y^2, \tag{20}$$

where

$$u_{sh}(x) = (\bar{V}_{||i}^{+} + \bar{V}_{||i}^{-})/2 \tag{21}$$

represents the asymmetry in the poloidal profile of $\bar{V}_{||i}$ that is introduced by the sheath boundary conditions. The only unconstrained Taylor coefficient is then $u_0(x)$. An equation for $u_0(x)$ can be obtained by inserting Eq. (17) into Eq. (15), which leads to

$$-\lambda^2\frac{\partial^2 u_0}{\partial x^2} + \frac{\lambda^2}{2L_T}\frac{\partial u_0}{\partial x} = u_0^{\infty} - u_0\ , \tag{22}$$

where

$$u_0^{\infty} = \frac{\sigma_\theta\sigma_\varphi}{\alpha|B_\varphi|}\frac{\partial\phi_0}{\partial x} - \frac{\sigma_\theta p_1}{m_i n_0|u_1|}, \tag{23}$$

and

$$\lambda = \sqrt{D_{turb}/\alpha|u_1|}\ . \tag{24}$$

We are thus left with a one-dimensional differential equation for $u_0(x)$, Eq. (22), which represents the momentum balance at the zeroth order in $y$.

Equation (22) can be solved analytically assuming that both $u_0^{\infty}$ and $\lambda$ remain about constant along $x$. The use of these rough assumptions allows revealing the interplay between the different mechanisms driving toroidal rotation. Under these assumptions, in fact, the solution of Eq. (22) that is regular at $x\to\infty$ is

$$u_0(x) = (u_0^s - u_0^{\infty})e^{-x/l} + u_0^{\infty}, \tag{25}$$

where we impose $u_0^s = u_0(0)$ at the separatrix, and

$$l = \frac{\lambda^2}{4L_T} + \sqrt{\lambda^2 + \left(\frac{\lambda^2}{4L_T}\right)^2}\ . \tag{26}$$

For typical SOL parameters, $\lambda \sim L_T$ and therefore $l \sim L_T$. Equations (19), (20), and (25), provide the expression of $u_0$, $u_1$, and $u_2$ in Eq. (17), and thus of the function $\bar{V}_{||i}(x,y)$, once $u_0^s$, $u_0^{\infty}$, and $u_{sh}$ are known.

An estimate of $u_{sh}$ can be obtained by assuming $T_e = T_0$, $T_i = \tau T_0$, and a potential of the order of the sheath potential barrier $e\phi_0 \approx \Lambda T_0$. Here, $T_0 \sim e^{-x/L_T}$ is the lowest order coefficient in the Taylor expansion of $T_e$, akin to that in Eq. (17). This gives

$$u_{sh} \sim -\sigma_\theta\sigma_\varphi\frac{\Lambda}{(1+\tau)\alpha}\frac{\rho_{s0}}{L_T}c_{s0}\,, \tag{27}$$

where $c_{s0} = \sqrt{T_0(1+\tau)/m_i}$.

An estimate of $u_0^{\infty}$ can be obtained as follows. The pressure poloidal asymmetry in Eq. (23) can be written as $p_1/(m_i n_0|u_1|) = c_{s0}(\delta n + \delta T)/2$, where $\delta n = (n_1/n_0)L_y$ and similarly for $\delta T$. Assuming for example that $n_1 \sim (n^+ - n^-)/L_y$, we can estimate $\delta n$ as the normalized density difference between the two divertor legs or limiter sides, namely $\delta n = (n^+ - n^-)/n_0$, and similarly for $\delta T$. This gives

$$u_0^{\infty} \sim u_{sh} - \frac{\sigma_\theta}{2}(\delta n + \delta T)c_{s0}\,. \tag{28}$$

On the other hand, the value of $u_0^s$ cannot be justified solely from SOL physics; a consistent choice should arise from the matching of the solution of Eq. (15) with the toroidal rotation profile in the closed-flux surface region. We remark that an equivalent situation is encountered when studying rotation in the closed flux surface region.[49,50] In the following, we explicit the solution of Eq. (15) and discuss a number of implications that are independent of the choice of $u_0^s$.

In order to easily interpret the toroidal plasma rotation resulting from Eq. (15), we consider the function

$$M = -\sigma_\theta\sigma_\varphi\frac{\bar{V}_{||i}}{c_{s0}}\,, \tag{29}$$

which is the parallel Mach number projected in the toroidal direction along the plasma current $I_p$, such that $M > 0$ always

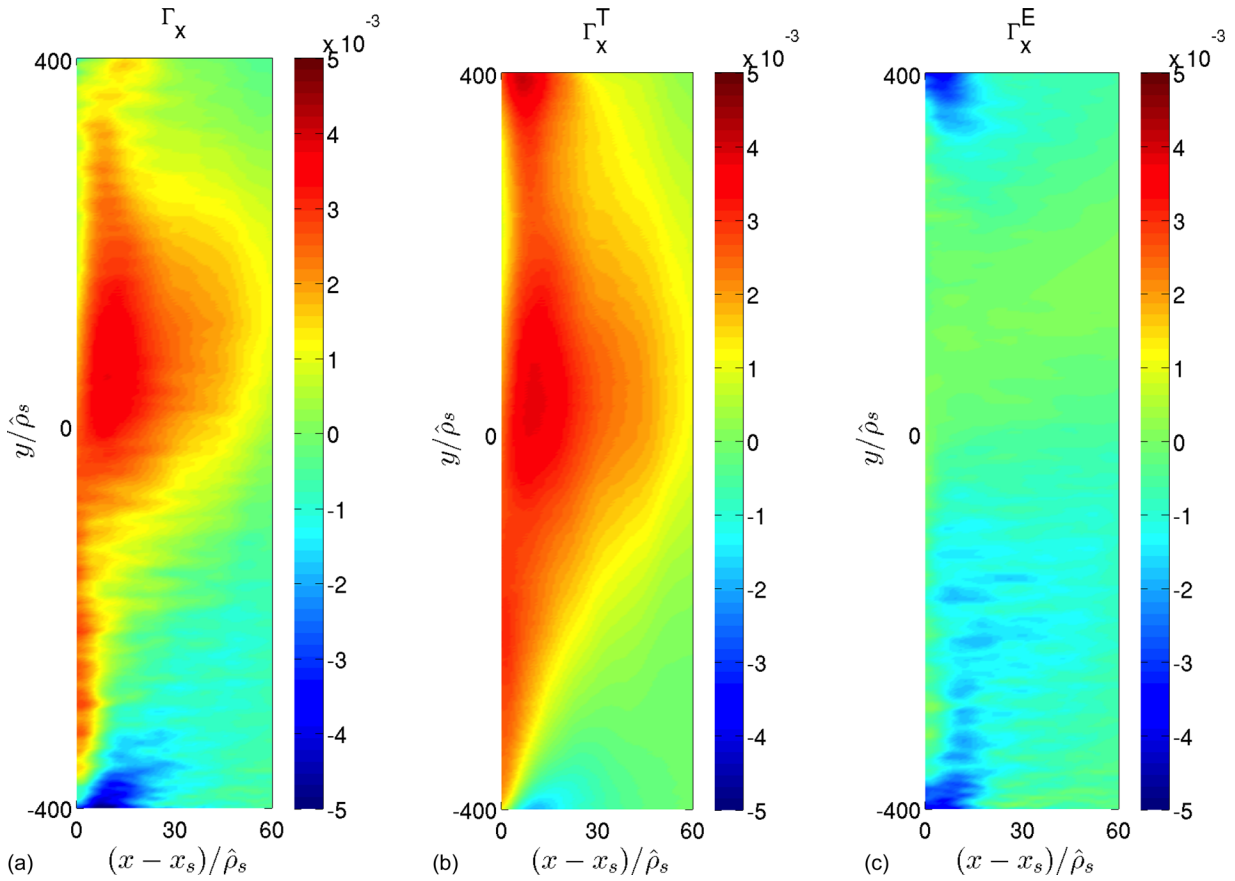


FIG. 6. Time-averaged radial momentum flux in the unfolded poloidal plane, computed from GBS simulation results with the limiter on the HFS. (a) $\bar{\Gamma}_x$ as defined in Eq. (7), (b) its turbulent component $\Gamma_x^T$, and (c) its equilibrium component $\Gamma_x^E$.

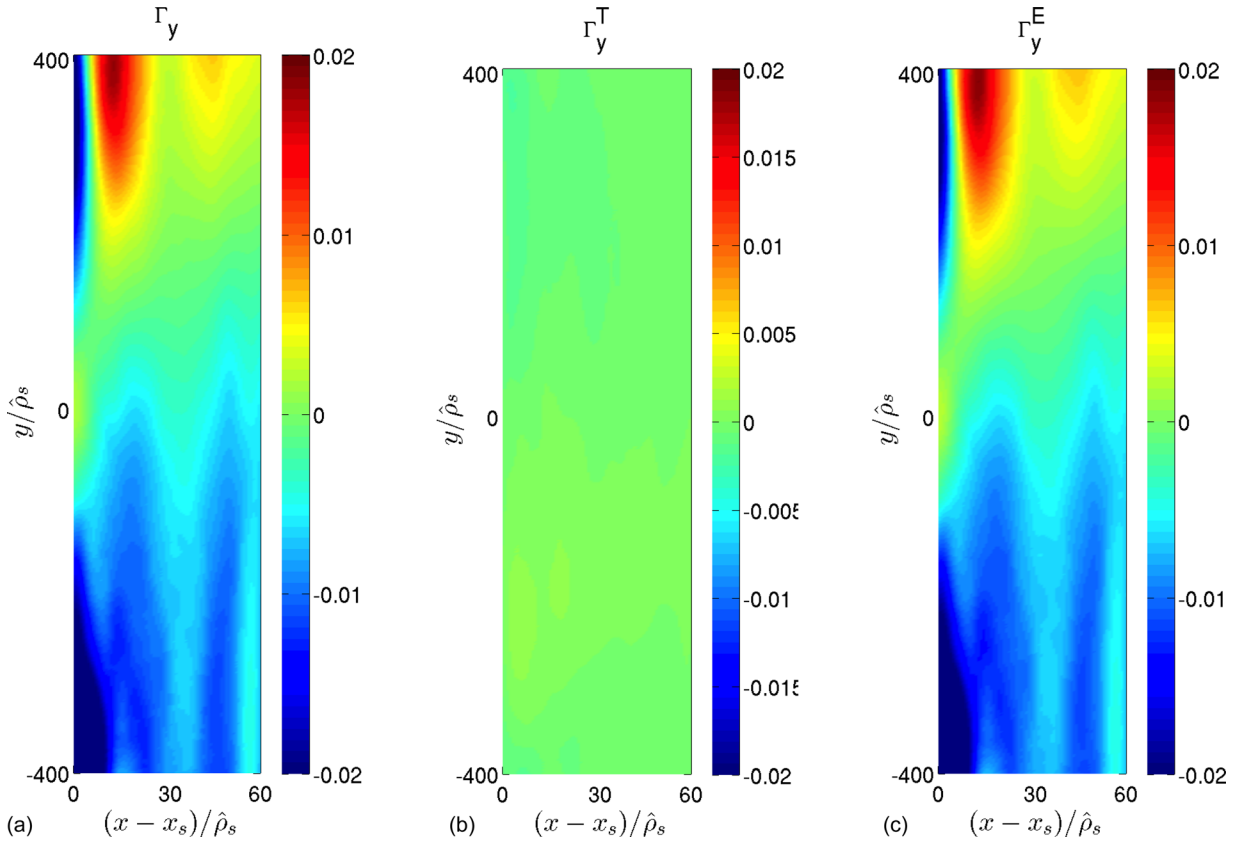


FIG. 7. Time-averaged poloidal momentum flux in the unfolded poloidal plane, computed from GBS simulation results with the limiter on the HFS. (a) $\bar{\Gamma}_y$ as defined in Eq. (7), (b) its turbulent component $\Gamma_y^T$, and (c) its equilibrium component $\Gamma_y^E$.

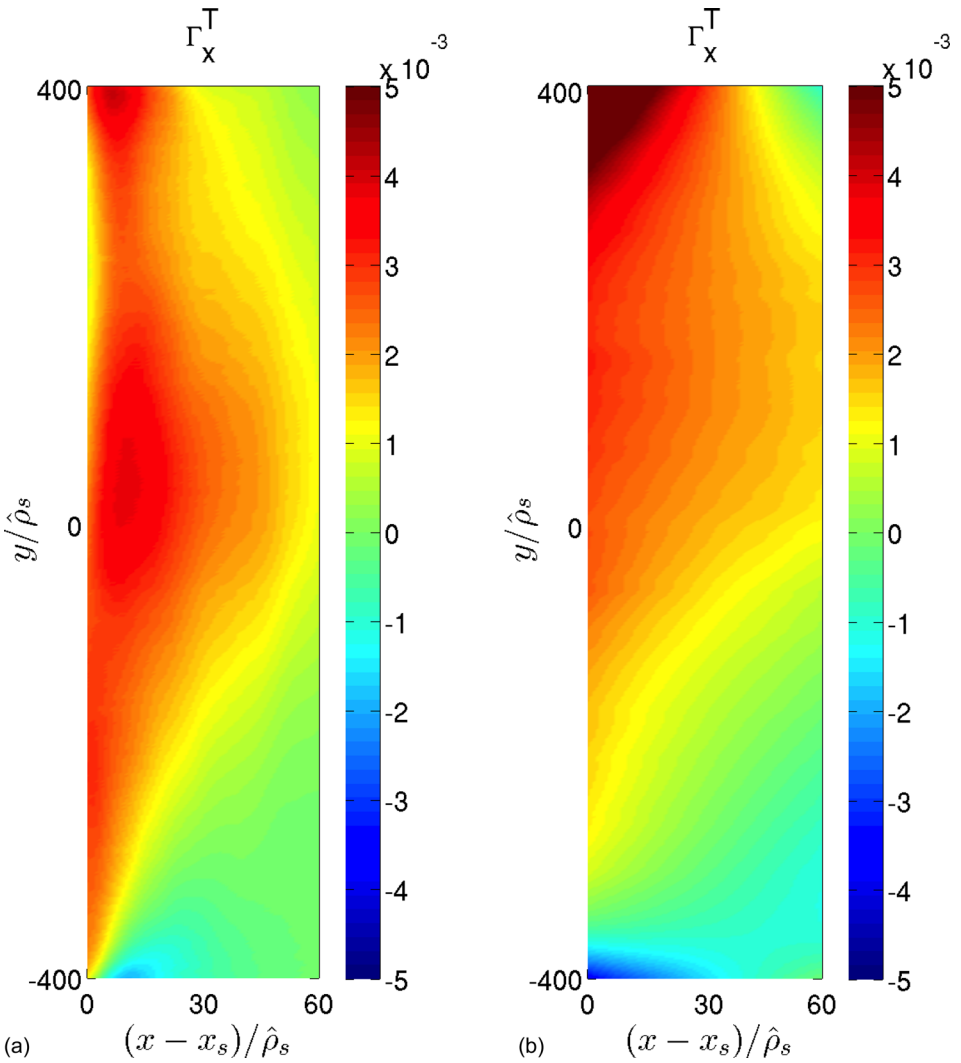


FIG. 8. Time-average of the turbulent radial momentum flux $\Gamma_x^T$ in the unfolded poloidal plane, computed from (a) GBS simulation results, and (b) the theoretical prediction as given by Eq. (13).

means co-current toroidal rotation. The approximate solution of Eq. (15) gives

$$M(x,y) = M_s e^{-x/l} + (M_{sh}+M_a)(1-e^{-x/l}) - 2\sigma_\varphi \frac{y}{L_y} + 4\left[(M_{sh}+M_a-M_s)e^{-x/l} - M_a\right]\frac{y^2}{L_y^2}, \quad (30)$$

where $M_s = M(0,0) = -\sigma_\theta \sigma_\varphi u_0^s / c_{s0}$ is the toroidal Mach number at the separatrix half way between the two limiter sides or divertor legs, $M_{sh} = \Lambda\rho_{s0}/(\alpha(1+\tau)L_T) \sim e^{-x/2L_T}$ represents the effect of the sheath on plasma rotation, and $M_a = \sigma_\varphi(\delta n + \delta T)/2$ is due to the pressure poloidal asymmetry. We remark that the sheath physics determines the value of $M_{sh}$ by setting both the ion flow $\bar{V}_{||i}$ at the boundaries and the radial electric field $\partial_x\phi$ in the main plasma. Also, the term $M_{sh}$ is always positive regardless of the magnetic field configuration, while the term $M_a$ may be positive or negative and therefore contribute to counter-current toroidal flows, as we shall see later.

Equation (30) is an analytical expression for the toroidal Mach number in the poloidal plane. We notice that since we did not solve the ion continuity equation, our prediction requires the knowledge of the density and temperature at the end of the field lines, i.e., $\delta n$ and $\delta T$. However, these are typically measured in tokamaks[23] and hence it is possible to compare the prediction of Eq. (30) with experimental measurements. But first, let us make a comparison with the GBS simulation results, in order to assess the validity of the theoretical model derived herein.

## IV. COMPARISON WITH SOL TURBULENCE SIMULATIONS

In this section, we compare some of the main assumptions and theoretical predictions derived in Sec. III with the results of GBS simulations carried out in a relatively simple configuration, i.e., the limited configuration described in Sec. II. We will consider four different limiter positions, namely, on the HFS midplane, on the low field side (LFS) midplane, and on the top and bottom of the vessel.

We start by considering the time-averaged radial and poloidal momentum fluxes, $\bar{\Gamma}_x$ and $\bar{\Gamma}_y$, as defined in Eq. (7). In Sec. III, we assumed that the radial flux is mainly due to turbulence while the poloidal flux is mainly due to equilibrium convection, namely $\bar{\Gamma}_x \simeq \Gamma_x^T$ and $\bar{\Gamma}_y \simeq \Gamma_x^E$. Figure 6 shows the profile of $\bar{\Gamma}_x$ in the unfolded poloidal plane, together with its components $\Gamma_x^T$ and $\Gamma_x^E$, for the HFS-limited case. The largest contribution to $\bar{\Gamma}_x$ clearly comes from $\Gamma_x^T$, except for the region close to the limiter plates, where the

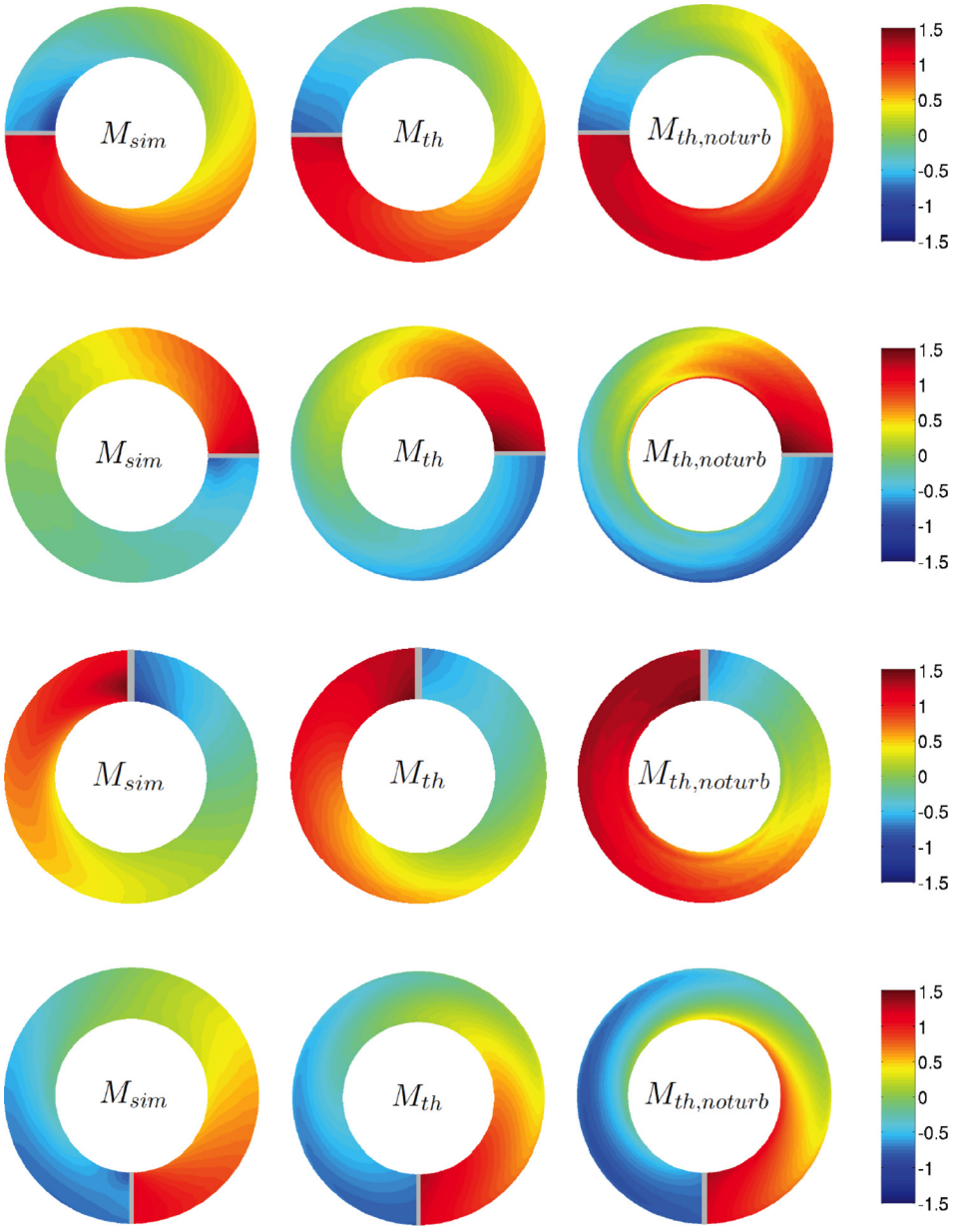


FIG. 9. Poloidal profile of the time-averaged Mach number $M(x, y)$, for a limiter on the HFS (first row), on the LFS (second row), on the top (third row) and on the bottom (last row). From GBS simulations (left column), as given by the prediction of Eq. (30) (middle column), and as given by Eq. (30) in the limit of $D_{turb} \to 0$ (right column).

presheath electric field, which is in the poloidal direction, produces an $\mathbf{E} \times \mathbf{B}$ flow in the radial direction. We can nevertheless conclude that the assumption $\bar{\Gamma}_x \simeq \Gamma_x^T$ is reasonable in most of the domain. Figure 7 shows the profile of $\bar{\Gamma}_y$ in the unfolded poloidal plane, together with its components $\Gamma_y^T$ and $\Gamma_y^E$, for the same simulation. The turbulent component is negligible and hence the assumption $\bar{\Gamma}_y \simeq \Gamma_y^E$ is very good. The same conclusions apply to the other limiter configurations (data not shown).

We now focus on the estimate of the turbulent momentum flux, $\Gamma_x^T$, which we assumed to result from the net transport arising from saturated turbulence, Eq. (13). Figure 8 shows the theoretical prediction for $\Gamma_x^T$ as given by Eq. (13), and compares it to the value obtained from GBS simulation results in the HFS-limited case. The agreement is rather good, and the same conclusion applies to the other limiter configurations (data not shown).

Finally, we consider the equilibrium Mach number $M(x, y)$ as defined in Eq. (29). Figure 9 shows the corresponding profile of $M(x, y)$ and its analytical prediction given by Eq. (30), for the four limiter positions. The agreement is generally rather good, as the prediction captures both the magnitude and the radial and poloidal structure of the Mach number. For comparison, the profile of $M(x, y)$ as given by Eq. (30) in the limit of no turbulence, i.e., taking $D_{turb} \to 0$, is also shown. This emphasizes the importance of the turbulent momentum transport in the description of the equilibrium rotation profiles. In particular, the volume-

TABLE I. Volume-averaged Mach number, $\langle M \rangle_{x,y}$, for different limiter positions and as given by the simulation results (left column), from Eq. (30) (middle column), and from Eq. (30) in the limit $D_{turb} \to 0$.

| | $\langle M_{sim} \rangle_{x,y}$ | $\langle M_{th} \rangle_{x,y}$ | $\langle M_{th,noturb} \rangle_{x,y}$ |
|---|---|---|---|
| LFS | 0.12 | 0.08 | 0.02 |
| HFS | 0.30 | 0.32 | 0.53 |
| TOP | 0.26 | 0.36 | 0.65 |
| BOT | 0.05 | 0.05 | −0.06 |

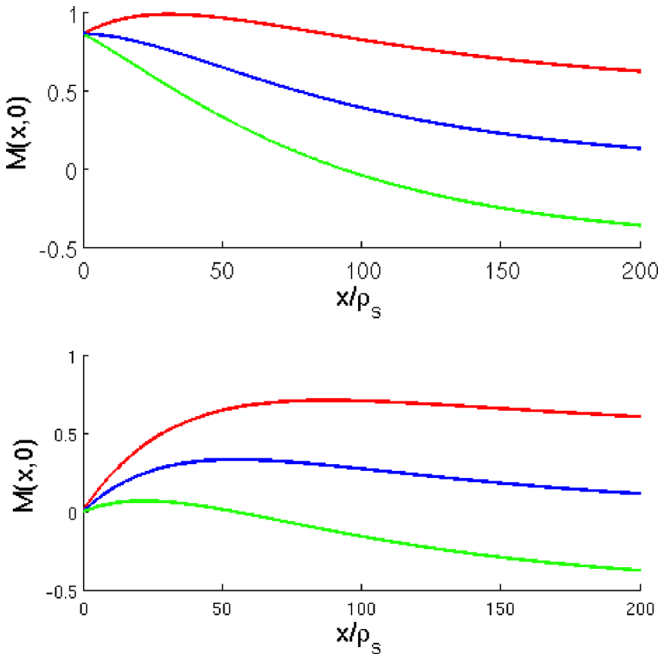


FIG. 10. Profile of $M(x, 0)$ as given by Eq. (30), for $\sigma_\varphi \delta n = 0.25$ (red), $\sigma_\varphi \delta n = 0$ (blue), and $\sigma_\varphi \delta n = -0.25$ (green). Top is for $M_s = M_{sh}(0)$ and bottom is for $M_s = 0$. Here $\alpha = 2^\circ$ and $l = L_T = 50\rho_s$.

averaged Mach number, $\langle M \rangle_{x,y}$, is only well reproduced when using Eq. (30) with the appropriate value of $D_{turb}$, as shown in Table I.

We conclude this section by discussing the main possible sources of discrepancy between the simulated Mach number and its theoretical prediction given by Eq. (30). First, the equilibrium component of the radial momentum flux, Eq. (7), has been neglected. However, as shown in Fig. 6, its contribution may become important in the vicinity of the limiter. Second, the Taylor expansion of the equilibrium ion parallel velocity, Eq. (17), is not always very accurate, especially when the poloidal asymmetries are strong. Considering higher order terms in the expansion may require to solve the continuity equation and to take into account the poloidal dependence of the turbulence drive, e.g., considering that $D_{turb} = D_{turb}(\theta)$. Third, Eq. (22) has been solved analytically by assuming that its right hand side is about constant, although it has a radial dependence. Finally, the term related to the effect of the sheath, Eq. (22), has been computed by assuming that the radial electric field has no poloidal dependence. However, as discussed in Ref. 31, this is in general not true. In fact, strong poloidal asymmetries yield significantly different radial electric fields at the two sides of the limiter.

TABLE II. Time and volume-averaged Mach number, $\langle M \rangle_{x,y}$, for different limiter positions and the corresponding sign of $\delta n$. For all cases $\sigma_\varphi = 1$.

| | $\langle M_{sim} \rangle_{x,y}$ | $\delta n$ |
|---|---|---|
| LFS | 0.12 | $<0$ |
| HFS | 0.30 | $>0$ |
| TOP | 0.26 | $>0$ |
| BOT | 0.05 | $<0$ |

## V. COMPARISON WITH EXPERIMENTAL TRENDS

In this section, we show that the estimate of the toroidal Mach number profile given by Eq. (30) provides an explanation for the observed experimental trends for the toroidal rotation in the SOL of tokamaks.

First of all, the direction of the toroidal rotation is typically measured to be in the co-current direction, even when the toroidal magnetic field[26] or the total magnetic field[23] is reversed. This is captured by the term $M_{sh} > 0$ in Eq. (30) which always contributes to co-current flow regardless of the sign of **B**. Moreover, we can estimate the magnitude of the toroidal rotation, which is typically measured to be $M \lesssim 1$.

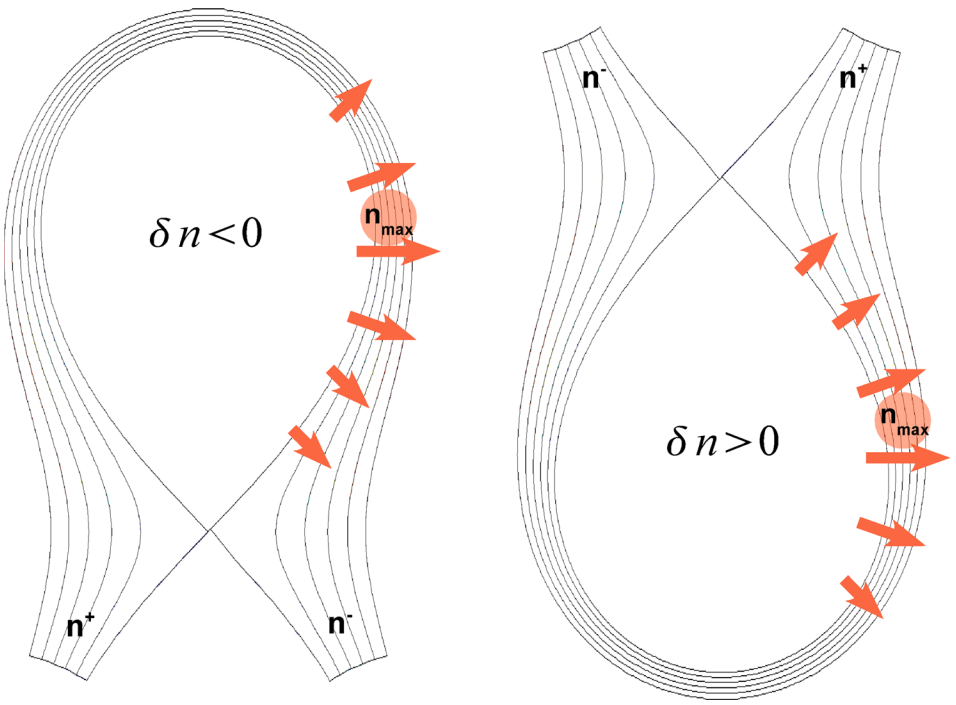


FIG. 11. The effect of the ballooned transport on the poloidal pressure asymmetry. The maximum of the density is always around the LFS. Depending on the limiter or divertor position, this gives $\delta n \sim (n^+ - n^-) < 0$ (left) or $\delta n \sim (n^+ - n^-) > 0$ (right).

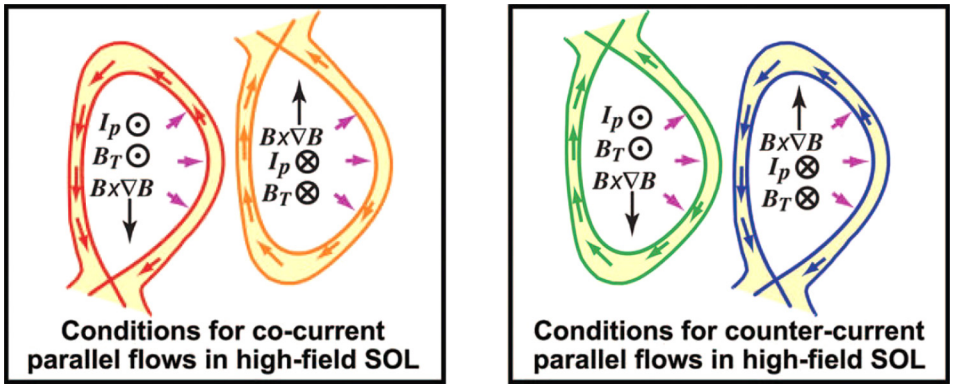


FIG. 12. Cartoon drawings of X-point topologies, field directions, and poloidal projections of the parallel flows measured in the high field side SOL. Reprinted with permission from.[23] Copyright 2008, AIP Publishing LLC.

Taking typical SOL parameters, e.g., $\Lambda = 3$, $\alpha = 0.03 \simeq 2^\circ$ and $\rho_s/L_T = 10^{-2}$,[21] we get $M_{sh} \simeq 0.5$.

It has been observed, nevertheless, that the magnitude and direction of toroidal rotation are not always exactly the same when reversing the magnetic field: rotation can become stronger or weaker in the co-current direction,[23,26] and under certain conditions it can even become counter-current.[27] We now show that this can be explained by the term $M_a \sim \sigma_\varphi \delta n$ in Eq. (30), which represents the effect of a pressure poloidal asymmetry. Far from the two divertor legs, $y/L_y \ll 1$, $M_a$ gives a co-current contribution if $\sigma_\varphi \delta n > 0$ and a counter-current contribution if $\sigma_\varphi \delta n < 0$. The effect of this term is illustrated in Fig. 10 where the function $M(x, 0)$ is shown for different values of $\sigma_\varphi \delta n$, and for two different values of $M_s$, showing that the choice of the latter does not affect the trends explored here. This effect explains the differences in the net toroidal flow observed between SOL simulations with different limiter positions. As Table II shows, in fact, the net co-current toroidal flow is stronger when $\delta n > 0$ and weaker when $\delta n < 0$ ($\sigma_\varphi = 1$ in all cases). The mechanism responsible for the sign of $\delta n$ is, as a matter of fact, the ballooning character of turbulent transport, which leads to a larger plasma pressure around the low field side, as sketched in Fig. 11. Thus, the sign of $\delta n$ depends on the relative position of the limiter or divertor with respect to the poloidal location of the pressure peak.

In a tokamak, if the plasma is diverted with a single null, one expects $\delta n < 0$ for a lower X-point and $\delta n > 0$ for an upper X-point (see Fig. 11), two configurations that have been explored in Alcator C-Mod.[27] As summarized in Fig. 12, in this tokamak it was concluded that favourable co-current situations in the SOL of L-mode plasmas are those with *normal B, lower single null* ($\sigma_\varphi < 0$, $\delta n < 0$) and *reversed B, upper single null* ($\sigma_\varphi > 0$, $\delta n > 0$). Similarly, favourable counter-current situations are those with *normal B, upper single null* ($\sigma_\varphi < 0$, $\delta n > 0$) and *reversed B, lower single null* ($\sigma_\varphi > 0$, $\delta n < 0$). Therefore these observations are all consistent with the contribution of the term $M_a \sim \sigma_\varphi \delta n$. Similarly, this model may be used to explain the trends observed in the SOL of other tokamaks, e.g., the TCV tokamak[26] or the Tore Supra tokamak.[51]

## VI. CONCLUSIONS AND OUTLOOK

In this paper, we have presented a first-principle based analytical theory to describe the generation and transport of toroidal plasma rotation in the SOL. As expected, the sources of intrinsic toroidal rotation reside at the boundary. The presence of the sheath, equilibrium poloidal $\mathbf{E} \times \mathbf{B}$ flows and pressure poloidal asymmetries can explain the local generation of toroidal rotation, which is radially transported by turbulence. The sheath physics naturally leads to a co-current toroidal rotation, while the effect of the poloidal pressure asymmetry (also regulated by the plasma-sheath interaction) can explain the flow reversals observed in tokamaks. Such flow reversals may occur when either the magnetic field or the limiter/divertor position are reversed, and this is explained by the ballooning character of the turbulence. Our theoretical predictions agree rather well with three-dimensional simulations of SOL turbulence.

The main limitation of our model is that ionization and recombination processes, which may affect the poloidal profile of $\bar{V}_{||i}$, are not taken into account. This may restrict the validity of the presented results to low-recycling regimes. Also, the theory derived herein ceases to be valid in regimes where turbulence is significantly suppressed and Pfirsch-Schlüter ion flows may play an important role, in particular in modulating the poloidal profile of the parallel ion velocity.

## ACKNOWLEDGMENTS

We acknowledge useful discussions with A. Bortolon, P. Catto, A. Fasoli, I. Furno, B. LaBombard, F. Parra, and C. Theiler. This work was supported in part by the Swiss National Science Foundation. Part of the simulations presented herein were carried out at the Swiss National Supercomputing Centre (CSCS) under project ID s346; and part were carried out using the HELIOS supercomputer system at Computational Simulation Centre of International Fusion Energy Research Centre (IFERC-CSC), Aomori, Japan, under the Broader Approach collaboration between Euratom and Japan, implemented by Fusion for Energy and JAEA.

## APPENDIX A: GBS EQUATIONS

The drift-reduced Braginskii equations[36] implemented in the GBS code describe the time-evolution of the plasma density, $n$, the vorticity, $\omega$, the electrostatic potential, $\phi$, the ion and electron parallel velocities, $V_{||i}$ and $V_{||e}$, and the electron temperature $T_e$.

With the definition of the Poisson bracket $\{f, g\}$ and the curvature operator $C(f)$,

$$\{f,g\} \equiv \mathbf{b}\cdot(\nabla f \times \nabla g), \tag{A1}$$

$$C(f) \equiv \frac{B}{2}\left(\nabla \times \frac{\mathbf{b}}{B}\right)\cdot \nabla f, \tag{A2}$$

where $B$ is the magnetic field strength and $\mathbf{b} = \mathbf{B}/B$, the drift-reduced Braginskii equations in the electrostatic, cold ion limit are

$$\frac{\partial n}{\partial t} = -\frac{1}{B}\{\phi, n\} - \nabla_\parallel (n V_{\parallel e}) + \frac{2}{eB}[C(p_e) - enC(\phi)] + S_n, \tag{A3}$$

$$\frac{en}{B\omega_{ci}}\frac{\partial \omega}{\partial t} = -\frac{en}{B\omega_{ci}}\{\phi,\omega\} - \frac{en}{B\omega_{ci}}V_{\parallel i}\nabla_\parallel \omega + \nabla_\parallel j_\parallel + \frac{2e}{B}C(p_e), \tag{A4}$$

$$m_e n\frac{\partial V_{\parallel e}}{\partial t} = -m_e n\frac{1}{B}\{\phi, V_{\parallel e}\} - m_e n V_{\parallel e}\nabla_\parallel V_{\parallel e} - \nabla_\parallel p_e + en\nabla_\parallel \phi - 0.71 n\nabla_\parallel T_e + en\nu_\parallel j_\parallel - \frac{4}{3}\eta_{0e}\nabla_\parallel^2 V_{\parallel e} - \frac{2\eta_{0e}}{3eB}\nabla_\parallel\left(5C(T_e) + 5\frac{T_e}{n}C(n) + eC(\phi)\right), \tag{A5}$$

$$m_i n\frac{\partial V_{\parallel i}}{\partial t} = -m_i n\frac{1}{B}\{\phi, V_{\parallel i}\} - m_i n V_{\parallel i}\nabla_\parallel V_{\parallel i} - \nabla_\parallel p_e, \tag{A6}$$

$$\frac{\partial T_e}{\partial t} = -\frac{1}{B}\{\phi, T_e\} - V_{\parallel e}\nabla_\parallel T_e - \frac{2}{3}T_e\nabla_\parallel V_{\parallel e} + 0.71\frac{2}{3}\frac{T_e}{en}\nabla_\parallel j_\parallel + \frac{2}{3n}\chi_{\parallel e}\nabla_\parallel^2 T_e + \frac{4}{3}\frac{1}{eB}\left[\frac{7}{2}T_e C(T_e) + \frac{T_e^2}{n}C(n) - eT_e C(\phi)\right] + S_T, \tag{A7}$$

which are coupled to the Poisson equation $\nabla_\perp^2\phi = \omega$. Here, $\omega_{ci} = eB/m_i$ is the ion gyrofrequency, $\nu_\parallel$ is the parallel Spitzer resistivity, $\chi_{\parallel e}$ is the electron parallel heat diffusivity, and $\eta_{0e}$ is the electron viscosity.[52] Also, $S_n$ and $S_T$ are the density and temperature sources, and $j_\parallel = en(V_{\parallel i} - V_{\parallel e})$ is the parallel current. We remark that the Poisson brackets are all of the form $\{\phi, f\}$ and represent the convection of the quantity $f$ with the $\mathbf{E}\times\mathbf{B}$ drift. The terms containing the curvature operator $C(f)$ arise from the divergence of the $\mathbf{E}\times\mathbf{B}$ and diamagnetic drifts, which is non-vanishing for a non-uniform magnetic field.

The coordinate system is as follows. We define $z$ as the parallel coordinate and we denote the perpendicular coordinates with $x$ and $y$, being $x$ the radial coordinate, and $y$ the coordinate perpendicular to both $x$ and the magnetic field (Figure 1). The coordinate system is such that $(y, x, z)$ is right-handed. For tokamak SOL electrostatic turbulence with circular magnetic flux surfaces, no magnetic shear, and a large aspect ratio, we have

$$C = \frac{1}{R}\left(\sin\theta\frac{\partial}{\partial x} + \cos\theta\frac{\partial}{\partial y}\right), \tag{A8}$$

$$\{f,g\} = \frac{\partial f}{\partial y}\frac{\partial g}{\partial x} - \frac{\partial g}{\partial y}\frac{\partial f}{\partial x}, \tag{A9}$$

$$\nabla_\perp^2 = \frac{\partial^2}{\partial x^2} + \frac{\partial^2}{\partial y^2}, \tag{A10}$$

$$\nabla_\parallel = \frac{\partial}{\partial z}, \tag{A11}$$

where $\theta$ is the poloidal angle defined such that $\theta = 0$ at the low-field-side midplane. Since $\alpha \ll 1$, the $(x, y)$ plane almost coincides with the poloidal plane $(x, \theta)$.

The GBS model equations, Eqs. (A3)–(A7), are completed with a set of boundary conditions at the end of the field lines, as given by the magnetic presheath entrance condition[32]

$$V_{\parallel i} = c_s\left[\pm 1 + \theta_n \mp \frac{1}{2}\theta_{T_e} - 2\frac{e\phi}{T_e}\theta_\phi\right], \tag{A12}$$

$$V_{\parallel e} = c_s\left[\pm\exp(\Lambda - e\phi/T_e) - 2\frac{e\phi}{T_e}\theta_\phi + 2(\theta_n + \theta_{T_e})\right], \tag{A13}$$

$$\frac{\partial \phi}{\partial y} = -\frac{m_i c_s}{e}\left[\pm 1 + \theta_n \pm \frac{1}{2}\theta_{T_e}\right]\frac{\partial V_{\parallel i}}{\partial y}, \tag{A14}$$

$$\frac{\partial n}{\partial y} = -\frac{n}{c_s}\left[\pm 1 + \theta_n \pm \frac{1}{2}\theta_{T_e}\right]\frac{\partial V_{\parallel i}}{\partial y}, \tag{A15}$$

$$\frac{\partial T_e}{\partial y} = e\kappa_T\frac{\partial \phi}{\partial y}, \tag{A16}$$

$$\nabla_\perp^2\phi = -\frac{m_i}{e}\left[(1+\theta_{T_e})\left(\frac{\partial V_{\parallel i}}{\partial y}\right)^2 + c_s\left(\pm 1 + \theta_n \pm \theta_{T_e}/2\right)\frac{\partial^2 V_{\parallel i}}{\partial y^2}\right], \tag{A17}$$

where the upper signs apply if the magnetic field is directed towards the wall, the lower signs apply in the opposite case. Here $\Lambda = \log(\sqrt{m_i/2\pi m_e})$ and in the GBS geometry

$$\theta_f = -\frac{\rho_s}{2\tan\alpha}\frac{\partial_x f}{f}, \tag{A18}$$

where $\rho_s = c_s/\omega_{ci}$. We remark that the electrostatic potential $\phi$ in Eq. (A13) is measured with respect to the wall potential, which is assumed to be zero. Also, the temperature gradient is very small since $\kappa_T \approx 0.1$ (see Ref. 32).

Finally, GBS works with normalized quantities defined through a reference temperature $\hat{T}_e$, a reference density $\hat{n}$, and a magnetic field $\hat{B}$. In particular, the electron temperature and the electrostatic potential are normalized such that $T_e \to T_e/\hat{T}_e$ and $\phi \to e\phi/\hat{T}_e$, and analogously for the density, $n \to n/\hat{n}$. The perpendicular coordinates are normalized with respect to $\hat{\rho}_s = \hat{c}_s/\hat{\omega}_{ci}$, where $\hat{c}_s = \sqrt{\hat{T}_e/m_i}$ and $\hat{\omega}_{ci} = e\hat{B}/m_i$. In the parallel direction, the macroscopic length $R$ is used. Finally, time is normalized such that $t \to t/(R/\hat{c}_s)$. The normalized system of equations evolved

by GBS can be found in Ref. 28. We remark that within this normalization, the parallel resistivity, heat diffusivity, and viscosity, are respectively normalized to $\hat{\nu} = m_i \hat{c}_s/(e^2 nR)$, $\hat{\chi} = n\hat{T}_e R/(\hat{c}_s m_i)$, and $\hat{\eta} = n\hat{T}_e (R/\hat{c}_s)(m_e/m_i)$.

## APPENDIX B: MOMENTUM CONSERVATION LAW

A conservation law for the ion momentum can be written within the drift-reduced Braginskii equations considered in the present paper. First, we notice that in the SOL of tokamaks, where the safety factor $q$ is large, the parallel direction almost coincides with the toroidal direction, and therefore one can assume $v_\parallel \simeq v_\varphi$. We therefore consider the ion momentum density in the parallel direction, $\pi_{\parallel i} = m_i n v_{\parallel i}$ (because of quasi neutrality, $n_i \simeq n$) and we evaluate

$$\frac{\partial \pi_{\parallel i}}{\partial t} + \nabla \cdot (\mathbf{v}_i \pi_{\parallel i}) = m_i v_{\parallel i} \left[ \frac{\partial n}{\partial t} + \nabla \cdot (n \mathbf{v}_i) \right] + m_i n \left[ \frac{\partial v_{\parallel i}}{\partial t} + (\mathbf{v}_i \cdot \nabla) v_{\parallel i} \right], \tag{B1}$$

where, according to the drift-reduced approximation, $\mathbf{v}_i = \mathbf{v}_{E\times B} + \mathbf{v}_{pol} + v_{\parallel i}\mathbf{b}$, being $\mathbf{v}_{E\times B} = \mathbf{b} \times \nabla\phi/B$ the $\mathbf{E}\times\mathbf{B}$ velocity and $\mathbf{v}_{pol}$ the ion polarization velocity (see, e.g., Ref. 36). The first term on the right hand side of Eq. (B1) can be evaluated by using the electron density equation, Eq. (A3), and the vorticity equation, Eq. (A4). In the source free region, the one of interest to investigate SOL turbulence and momentum transport, we find

$$m_i v_{\parallel i} \left[ \frac{\partial n}{\partial t} + \nabla \cdot (n \mathbf{v}_i) \right] = 0. \tag{B2}$$

For the second term on the right hand side of Eq. (B1), by neglecting $\mathbf{v}_{pol}$ with respect to $\mathbf{v}_{E\times B}$, as $v_{pol}/v_{E\times B} \sim (\rho_s/L_\perp)^2 \ll 1$ in the SOL, we have from the ion momentum equation, Eq. (A6), that

$$m_i n \left[ \frac{\partial v_{\parallel i}}{\partial t} + (\mathbf{v}_i \cdot \nabla) v_{\parallel i} \right] = -\nabla_\parallel p_e. \tag{B3}$$

By introducing Eqs. (B2) and (B3) into Eq. (B1), we find

$$\frac{\partial \pi_{\parallel i}}{\partial t} + \nabla \cdot (\mathbf{v}_i \pi_{\parallel i}) = -\nabla_\parallel p_e. \tag{B4}$$

We can therefore write a conservation law for the total ion parallel momentum, $\Pi_{\parallel i} = \int_V \pi_{\parallel i} d^3x$, by integrating Eq. (B4) over the SOL volume, obtaining

$$\frac{\partial \Pi_{\parallel i}}{\partial t} = -\int_V \nabla_\parallel p_e - \int_{\partial V} \pi_{\parallel i} \mathbf{v}_i \cdot d\mathbf{S}. \tag{B5}$$

Equation (B5) shows that the net sources of momentum in the SOL must come from the boundary. In fact, the first term on the right-hand-side of Eq. (B5) gives a surface-average of the pressure difference between the two ends of the field lines (namely, the two sides of the limiter or diverter legs). The second term has a contribution from the surface-averaged momentum outflow at the limiters and a contribution from the surface-averaged momentum inflow/outflow at the radial boundaries. This result implies that the source of intrinsic toroidal flow in the SOL is determined both by the flow and pressure differences at the boundaries, thus strongly regulated by the sheath physics.

## APPENDIX C: SCALING OF THE EQUILIBRIUM PRESSURE SCALE LENGTH

Within the drift-reduced fluid model, a pressure continuity equation can be obtained by combining the density and temperature equations, Eqs. (A3) and (A7). Assuming that the dominant terms are the parallel convection and the radial turbulent transport, we are left with an approximate pressure balance

$$\frac{\partial p}{\partial t} + \frac{\partial \Gamma_p}{\partial x} + \nabla_\parallel (p V_{\parallel e}) = 0\,, \tag{C1}$$

where $\Gamma_p = \tilde{p}\partial_y \tilde{\phi}/B$ is the turbulent radial flux of plasma pressure. Writing

$$\langle \partial_x \Gamma_p \rangle_t \sim \bar{\Gamma}_p / L_p \tag{C2}$$

and

$$\langle \nabla_\parallel (p V_{\parallel e}) \rangle_t \sim \bar{p} c_s / qR\,, \tag{C3}$$

the time-average of Eq. (C1) leads to

$$L_p \sim \frac{qR}{c_s} \frac{\bar{\Gamma}_p}{\bar{p}}. \tag{C4}$$

An estimate of $\bar{\Gamma}_p = \langle \tilde{p}\partial_y \tilde{\phi} \rangle_t / B$ can be obtained as follows. Linearizing Eq. (C1) and keeping the dominant terms, one has

$$\gamma \tilde{p} \sim \frac{1}{B} \frac{\partial \tilde{\phi}}{\partial y} \frac{\partial \bar{p}}{\partial x}, \tag{C5}$$

thus relating the electric field fluctuations with the pressure fluctuations. Therefore we have $\bar{\Gamma}_p \sim (\gamma L_p/\bar{p}) \langle \tilde{p}^2 \rangle_t$. Finally, we can relate $\tilde{p}$ with $\bar{p}$ by using the *gradient removal* hypothesis, namely by assuming that the mode growth saturates when the fluctuations are able to remove the instability drive, which is provided by the pressure gradient, i.e., when

$$\frac{\partial \tilde{p}}{\partial x} \sim \frac{\partial \bar{p}}{\partial x}\,. \tag{C6}$$

This condition can be written as $k_x \tilde{p} \sim \bar{p}/L_p$, where $k_x$ gives the radial extension of the saturated turbulent eddies. This can be estimated using non-local linear theory as $k_x = \sqrt{k_y/L_p}$.[40] We can therefore write

$$\langle \tilde{p}^2 \rangle_t \sim \frac{\bar{p}^2}{k_y L_p}\,. \tag{C7}$$

Hence, we are left with an expression for the radial pressure flux, $\bar{\Gamma}_p$, as a function of equilibrium quantities

$$\bar{\Gamma}_p \sim \bar{p}\left(\frac{\gamma}{k_y}\right)_{max}, \tag{C8}$$

where the linear growth rate $\gamma$ and the wavenumber $k_y$ must be chosen in order to maximize the ratio of $\gamma/k_y$, thus maximizing the transport. Finally, we can replace this expression into Eq. (C4), leading to

$$L_p \sim \frac{qR}{c_s}\left(\frac{\gamma}{k_y}\right)_{max}. \tag{C9}$$


[1]L.-G. Eriksson, E. Righi, and K.-D. Zastrow, "Toroidal rotation in ICRF-heated H-modes on JET," Plasma Phys. Control. Fusion **39**(1), 27–42 (1997).
[2]I. H. Hutchinson, J. Rice, R. Granetz, and J. Snipes, "Self-acceleration of a tokamak plasma during ohmic H mode," Phys. Rev. Lett. **84**(15), 3330–3333 (2000).
[3]A. Bortolon, B. Duval, A. Pochelon, and A. Scarabosio, "Observation of spontaneous toroidal rotation inversion in ohmically heated tokamak plasmas," Phys. Rev. Lett. **97**(23), 235003 (2006).
[4]A. Bondeson and D. Ward, "Stabilization of external modes in tokamaks by resistive walls and plasma rotation," Phys. Rev. Lett. **72**(17), 2709–2712 (1994).
[5]E. Strait, T. Taylor, A. Turnbull, J. Ferron, L. Lao, B. Rice, O. Sauter, S. Thompson, and D. Wróblewski, "Wall Stabilization of High Beta Tokamak Discharges in DIII-D," Phys. Rev. Lett. **74**(13), 2483–2486 (1995).
[6]P. Mantica, D. Strintzi, T. Tala, C. Giroud, T. Johnson, H. Leggate, E. Lerche, T. Loarer, A. Peeters, A. Salmi, S. Sharapov, D. Van Eester, P. de Vries, L. Zabeo, and K.-D. Zastrow, "Experimental study of the ion critical-gradient length and stiffness level and the impact of rotation in the jet tokamak," Phys. Rev. Lett. **102**(17), 175002 (2009).
[7]A. Eriksson, H. Nordman, P. Strand, J. Weiland, T. Tala, E. Asp, G. Corrigan, C. Giroud, M. de Greef, I. Jenkins, H. C. M. Knoops, P. Mantica, K. M. Rantamäki, P. C. de Vries, and K.-D. Zastrow, "Predictive simulations of toroidal momentum transport at JET," Plasma Phys. Control. Fusion **49**(11), 1931–1943 (2007).
[8]F. D. Halpern, A. H. Kritz, G. Bateman, A. Y. Pankin, R. V. Budny, and D. C. McCune, "Predictive simulations of ITER including neutral beam driven toroidal rotation," Phys. Plasmas **15**(6), 062505 (2008).
[9]A. Scarabosio, A. Bortolon, B. P. Duval, A. Karpushov, and A. Pochelon, "Toroidal plasma rotation in the TCV tokamak," Plasma Phys. Control. Fusion **48**(5), 663–683 (2006).
[10]J. S. de Grassie, "Tokamak rotation sources, transport and sinks," Plasma Phys. Control. Fusion **51**(12), 124047 (2009).
[11]B. P. Duval, A. Bortolon, A. Karpushov, R. A. Pitts, A. Pochelon, and A. Scarabosio, "Bulk plasma rotation in the TCV tokamak in the absence of external momentum input," Plasma Phys. Control. Fusion **49**(12B), B195–B209 (2007).
[12]S. H. Muller, J. A. Boedo, K. H. Burrell, J. S. de Grassie, R. A. Moyer, D. L. Rudakov, and W. M. Solomon, "Experimental investigation of the role of fluid turbulent stresses and edge plasma flows for intrinsic rotation generation in diii-d h-mode plasmas," Phys. Rev. Lett. **106**(11), 115001 (2011).
[13]Y. Camenen, A. Peeters, C. Angioni, F. Casson, W. Hornsby, A. Snodin, and D. Strintzi, "Transport of parallel momentum induced by current-symmetry breaking in toroidal plasmas," Phys. Rev. Lett. **102**(12), 125001 (2009).
[14]W. X. Wang, T. S. Hahm, S. Ethier, L. E. Zakharov, and P. H. Diamond, "Trapped electron mode turbulence driven intrinsic rotation in tokamak plasmas," Phys. Rev. Lett. **106**(8), 085001 (2011).
[15]A. G. Peeters, C. Angioni, A. Bortolon, Y. Camenen, F. J. Casson, B. Duval, L. Fiederspiel, W. A. Hornsby, Y. Idomura, T. Hein, N. Kluy, P. Mantica, F. I. Parra, A. P. Snodin, G. Szepesi, D. Strintzi, T. Tala, G. Tardini, P. de Vries, and J. Weiland, "Overview of toroidal momentum transport," Nucl. Fusion **51**(9), 094027 (2011).
[16]J. W. Connor and H. R. Wilson, "A review of theories of the L-H transition," Plasma Phys. Control. Fusion **42**(1), R1–R74 (2000).
[17]O. D. Gurcan, P. H. Diamond, C. J. McDevitt, and T. S. Hahm, "A simple model of intrinsic rotation in high confinement regime tokamak plasmas," Phys. Plasmas **17**(3), 032509 (2010).
[18]F. I. Parra, M. F. F. Nave, A. A. Schekochihin, C. Giroud, J. S. de Grassie, J. H. F. Severo, P. de Vries, and K.-D. Zastrow, "Scaling of spontaneous rotation with temperature and plasma current in tokamaks," Phys. Rev. Lett. **108**(9), 095001 (2012).
[19]T. Stoltzfus-Dueck, "Transport-driven toroidal rotation in the tokamak edge," Phys. Rev. Lett. **108**(6), 065002 (2012).
[20]N. Fedorczak, P. H. Diamond, G. Tynan, and P. Manz, "Shear-induced Reynolds stress at the edge of L-mode tokamak plasmas," Nucl. Fusion **52**(10), 103013 (2012).
[21]B. LaBombard, J. E. Rice, A. E. Hubbard, J. W. Hughes, M. Greenwald, J. Irby, Y. Lin, B. Lipschultz, E. S. Marmar, C. S. Pitcher, N. Smick, S. M. Wolfe, S. J. Wukitch, and the Alcator Group, "Transport-driven Scrape-Off-Layer flows and the boundary conditions imposed at the magnetic separatrix in a tokamak plasma," Nucl. Fusion **44**(10), 1047–1066 (2004).
[22]V. D. Pustovitov, "Integral torque balance in tokamaks," Nucl. Fusion **51**(1), 013006 (2011).
[23]B. LaBombard, J. W. Hughes, N. Smick, A. Graf, K. Marr, R. McDermott, M. Reinke, M. Greenwald, B. Lipschultz, J. L. Terry, D. G. Whyte, and S. J. Zweben, "Critical gradients and plasma flows in the edge plasma of Alcator C-Mod," Phys. Plasmas **15**(5), 056106 (2008).
[24]A. V. Chankin and W. Kerner, "Edge toroidal momentum and its effect on the scrape-off layer," Nucl. Fusion **36**(5), 563–569 (1996).
[25]V. A. Rozhansky, S. P. Voskoboynikov, E. G. Kaveeva, D. P. Coster, and R. Schneider, "Simulation of tokamak edge plasma including self-consistent electric fields," Nucl. Fusion **41**(4), 387–401 (2001).
[26]R. A. Pitts, J. Horacek, W. Fundamenski, O. E. Garcia, A. H. Nielsen, M. Wischmeier, V. Naulin, and J. Juul Rasmussen, "Parallel SOL flow on TCV," J. Nucl. Mater. **363–365**, 505–510 (2007).
[27]B. LaBombard, J. W. Hughes, D. Mossessian, M. Greenwald, B. Lipschultz, J. L. Terry, and the Alcator C-Mod Team, "Evidence for electromagnetic fluid drift turbulence controlling the edge plasma state in the Alcator C-Mod tokamak," Nucl. Fusion **45**(12), 1658–1675 (2005).
[28]P. Ricci, F. D. Halpern, S. Jolliet, J. Loizu, A. Mosetto, A. Fasoli, I. Furno, and C. Theiler, "Simulation of plasma turbulence in scrape-off layer conditions: The GBS code, simulation results and code validation," Plasma Phys. Control. Fusion **54**(12), 124047 (2012).
[29]H. R. Wilson, S. C. Cowley, A. Kirk, and P. B. Snyder, "Magneto-hydrodynamic stability of the H-mode transport barrier as a model for edge localized modes: An overview," Plasma Phys. Control. Fusion **48**(5A), A71–A84 (2006).
[30]J. T. Omotani and B. D. Dudson, "Non-local approach to kinetic effects on parallel transport in fluid models of the scrape-off layer," Plasma Phys. Control. Fusion **55**(5), 055009 (2013).
[31]J. Loizu, P. Ricci, F. D. Halpern, S. Jolliet, and A. Mosetto, "On the electrostatic potential in the scrape-off layer of magnetic confinement devices," Plasma Phys. Control. Fusion **55**(12), 124019 (2013).
[32]J. Loizu, P. Ricci, F. D. Halpern, and S. Jolliet, "Boundary conditions for plasma fluid models at the magnetic presheath entrance," Phys. Plasmas **19**(12), 122307 (2012).
[33]A. Mosetto, F. D. Halpern, S. Jolliet, J. Loizu, and P. Ricci, "Turbulent regimes in the tokamak scrape-off layer," Phys. Plasmas **20**(9), 092308 (2013).
[34]P. Ricci and B. N. Rogers, "Plasma turbulence in the scrape-off layer of tokamak devices," Phys. Plasmas **20**(1), 010702 (2013).
[35]B. Rogers, J. Drake, and A. Zeiler, "Phase space of tokamak edge turbulence, the l-h transition, and the formation of the edge pedestal," Phys. Rev. Lett. **81**(20), 4396–4399 (1998).
[36]A. Zeiler, J. F. Drake, and B. Rogers, "Nonlinear reduced Braginskii equations with ion thermal dynamics in toroidal plasma," Phys. Plasmas **4**, 2134 (1997).
[37]J. J. Ramos, "General expression of the gyroviscous force," Phys. Plasmas **12**(11), 112301 (2005).
[38]P. C. Stangeby, "The plasma boundary of magnetic fusion devices," Institute of Physics, Berkshire, 2000.
[39]C. Hidalgo, B. Gonçalves, C. Silva, M. Pedrosa, K. Erents, M. Hron, and G. Matthews, "Experimental investigation of dynamical coupling between turbulent transport and parallel flows in the jet plasma-boundary region," Phys. Rev. Lett. **91**(6), 065001 (2003).
[40]P. Ricci and B. N. Rogers, "Transport scaling in interchange-driven toroidal plasmas," Phys. Plasmas **16**(6), 062303 (2009).
[41]A. Mosetto, F. D. Halpern, S. Jolliet, and P. Ricci, "Low-frequency linear-mode regimes in the tokamak scrape-off layer," Phys. Plasmas **19**(11), 112103 (2012).
[42]F. D. Halpern, P. Ricci, B. Labit, I. Furno, S. Jolliet, J. Loizu, A. Mosetto, G. Arnoux, J. P. Gunn, J. Horacek, M. Kočan, B. LaBombard, and

C. Silva, "Theory-based scaling of the SOL width in circular limited tokamak plasmas," Nucl. Fusion **53**(12), 122001 (2013).
[43]J. Loizu, P. Ricci, F. D. Halpern, S. Jolliet, and A. Mosetto, "Effects of the limiter position on the scrape-off layer width, radial electric field and intrinsic flows," Nucl. Fusion (submitted).
[44]C. Silva, H. Figueiredo, P. Duarte, and H. Fernandes, "Characterization of the poloidal asymmetries in the ISTTOK edge plasma," Plasma Phys. Control. Fusion **53**(8), 085021 (2011).
[45]J. P. Gunn, C. Boucher, M. Dionne, I. Duran, V. Fuchs, T. Loarer, I. Nanobashvili, R. Pánek, J.-Y. Pascal, F. Saint-Laurent, J. Stöckel, T. Van Rompuy, R. Zagórski, J. Adámek, J. Bucalossi, R. Dejarnac, P. Devynck, P. Hertout, M. Hron, G. Lebrun, P. Moreau, F. Rimini, A. Sarkissian, and G. Van Oost, "Evidence for a poloidally localized enhancement of radial transport in the scrape-off layer of the tore supra tokamak," J. Nucl. Mater. **363–365**, 484–490 (2007).
[46]A. Aydemir, "Shear flows at the tokamak edge and their role in core rotation and the l-h transition," Phys. Rev. Lett. **98**(22), 225002 (2007).
[47]F. D. Halpern, S. Jolliet, J. Loizu, A. Mosetto, and P. Ricci, "Ideal ballooning modes in the tokamak scrape-off layer," Phys. Plasmas **20**(5), 052306 (2013).
[48]N. Asakura, "Understanding the SOL flow in L-mode plasma on divertor tokamaks, and its influence on the plasma transport," J. Nucl. Mater. **363–365**, 41–51 (2007).
[49]P. H. Diamond, C. J. McDevitt, Ö. D. Gürcan, T. S. Hahm, W. X. Wang, E. S. Yoon, I. Holod, Z. Lin, V. Naulin, and R. Singh, "Physics of non-diffusive turbulent transport of momentum and the origins of spontaneous rotation in tokamaks," Nucl. Fusion **49**(4), 045002 (2009).
[50]V. A. Rozhansky and I. Yu. Senichenkov, "1D equation for toroidal momentum transport in a tokamak," Plasma Phys. Control. Fusion **52**(6), 065003 (2010).
[51]N. Fedorczak, "Etude expérimentale du transport turbulent au bord d'un plasma de tokamak," Ph.D thesis, Université de Provence, 2010.
[52]S. I. Braginskii, *Transport Processes in a Plasma*, edited by M. A. Leontovich, Reviews of Plasma Physics, Vol. 1 (Consultants Bureau, New York, 1965), p. 205.